



1 **A Holocene temperature (brGDGT) record from Garba**  
2 **Guracha, a high-altitude lake in Ethiopia.**

3 Lucas Bittner<sup>1</sup>, Cindy De Jonge<sup>2</sup>, Graciela Gil-Romera<sup>3,4</sup>, Henry F. Lamb<sup>5,6</sup>, James M. Russell<sup>7</sup>,  
4 Michael Zech<sup>1</sup>

5 <sup>1</sup>) Heisenberg Chair of Physical Geography with focus on paleoenvironmental research, Institute of Geography,  
6 Technische Universität Dresden, Dresden, Germany

7 <sup>2</sup>) Geological Institute, Department of Earth Sciences, ETH Swiss Federal Institute of Technology, 8092 Zurich,  
8 Switzerland

9 <sup>3</sup>) Plant Ecology and Geobotany dept., Philipps-Marburg University, Marburg, Germany.

10 <sup>4</sup>) Department of Geo-environmental Processes and Global Change, Pyrenean Institute of Ecology, CSIC, Zaragoza,  
11 Spain

12 <sup>5</sup>) Department of Geography and Earth Sciences, Aberystwyth University, Aberystwyth, UK.

13 <sup>6</sup>) Department of Botany, School of Natural Sciences, Trinity College Dublin, Dublin 2, Ireland

14 <sup>7</sup>) Department of Geological Sciences, Brown University, USA

15 *Correspondence to:* Lucas Bittner ([lucas.bittner@tu-dresden.de](mailto:lucas.bittner@tu-dresden.de))

16

17

18

19

20

21

22

23



24 **Abstract.** Eastern Africa has experienced strong climatic changes since the last deglaciation (15,000 years ago). The  
25 driving mechanisms and teleconnections of these spatially complex climate variations are yet not fully understood.  
26 Although previous studies on lake systems have largely enhanced our knowledge of Holocene precipitation variation  
27 in eastern Africa, few such studies have reconstructed the terrestrial temperature history of eastern Africa from lake  
28 archives. Here, we present (i) a new branched glycerol dialkyl glycerol tetraether (brGDGT) temperature calibration  
29 that includes Bale Mountain surface sediments and (ii) a quantitative record of mean annual temperature (MAT) over  
30 the past 12 cal ka BP using brGDGTs in a sediment core collected from Garba Guracha (3950 m a.s.l.) in the Bale  
31 Mountains. After adding Bale Mountain surface sediment (n=11) data to the existing East African lake dataset,  
32 additional variation in 6-methyl brGDGTs was observed, which necessitated modifying the MBT'<sub>5ME</sub> calibration by  
33 adding 6-methyl brGDGT IIIa' (resulting in the MBT-Bale Mountain index,  $r^2=0.93$ ,  $p<0.05$ ). Comparing the MBT'<sub>5ME</sub>  
34 and the new MBT-Bale Mountain index, our high altitude Garba Guracha temperature record shows that significant  
35 warming occurred shortly after the Holocene onset. The temperature increased by more than 3.0 °C in less than 600  
36 years. The highest temperatures prevailed between 9 and 6 cal ka BP, followed by a temperature decrease until 1.4 cal  
37 ka BP. The reconstructed temperature history is strongly linked to supraregional climatic changes associated with  
38 insolation forcing and the African Humid Period (AHP), as well as with local anomalies associated with catchment  
39 deglaciation and hydrology.

40  
41 **Keywords:** paleolimnology; MAT; brGDGT, calibration, palaeoclimatology, eastern Africa

## 42 **1. INTRODUCTION**

43 The severity of the current climate change and its global implications have been widely discussed following the latest  
44 report from the Intergovernmental Panel for Climate Change (IPCC) (IPCC, 2021). This highlights the need for the  
45 scientific community to use palaeoclimate to estimate climate baseline conditions prior to human impact on climate  
46 (Neukom et al., 2019). Although palaeoclimatology has become a central discipline in understanding current climate  
47 variability (Thompson et al., 2002), important areas of the planet remain understudied. A partial understanding of  
48 global climate complexity can lead to biased views of natural systems (Hughes et al., 2021). This is the case for the  
49 African continent in general and northeastern Africa in particular. Current climatic conditions in eastern Africa vary  
50 significantly due to its complex topography and the influence of the Intertropical Convergence Zone (ITCZ), the Indian



51 Monsoon and the El Niño-Southern Oscillation (ENSO). All of these affect temperature and the distribution, amount  
52 and timing of rainfall in the region, resulting in a wide range of climatic conditions from the warm, dry and semi-arid  
53 conditions of northern Kenya, south-eastern Ethiopia, Djibouti and Somalia to the cool, humid conditions of the  
54 western highlands (Hove et al., 2011; Nicholson, 2017; Lyon and Vigaud, 2017).

55

56 There is clear evidence indicating that, since the last glacial period, northern and eastern Africa experienced severe  
57 climatic changes (Tierney et al., 2008, 2011a, 2017, 2013; Loomis et al., 2015; Wagner et al., 2018). Three major  
58 climate events are the post-glacial warming (~15 ka BP), the hydrological variability during the African Humid Period  
59 (AHP) (15 -5 ka BP) (deMenocal et al., 2000), that lead to the greening of the Saharan Desert (Blom et al., 2009), and  
60 the drying period at the beginning of the Meghalayan (4.2 ka BP) (Bini et al., 2019). The intensity and the timing of  
61 these climatic changes varied regionally over northern and eastern Africa (Castañeda et al., 2016). While the driving  
62 mechanisms and the regional differences are complex and not fully understood, evidence supports the view that  
63 climatic changes in northern and eastern Africa were connected across the northern hemisphere (Tierney et al., 2013;  
64 Tierney and Russell, 2007; Otto-Bliesner et al., 2014). These complex teleconnections and their global impact support  
65 the importance of understanding long-term climate drivers in eastern Africa. Such knowledge will lead to better  
66 assessments of the impacts and potential mitigation of the current and future climate change scenarios in this world's  
67 understudied yet critical region.

68 While several studies have reconstructed the precipitation history in Northern and eastern Africa over the last 15 cal  
69 ka BP (Bittner et al., 2021; Costa et al., 2014; Jaeschke et al., 2020; Junginger et al., 2014; Morrissey and Scholz,  
70 2014; Tierney et al., 2011a; Trauth et al., 2018; Wagner et al., 2018), only a few have reconstructed the regional  
71 temperature history in northeastern Africa (Castañeda et al., 2016; Morrissey et al., 2018; Berke et al., 2012a; Loomis  
72 et al., 2017, 2012, 2015; Tierney et al., 2008, 2016). Moreover, there is a lack of terrestrial temperature reconstructions,  
73 especially in the high altitudes and the Horn of Africa.

74 For terrestrial archives, different methods have been developed and applied based on pollen, chironomids, and lipid  
75 biomarkers (Cheddadi et al., 1998; Wu et al., 2007; Chevalier and Chase, 2015; Bonnefille et al., 1992; Eggermont et  
76 al., 2010; Schouten et al., 2007). Over the last 15 years, an innovative approach for temperature reconstructions  
77 emerged based on branched glycerol dialkyl glycerol tetraethers (brGDGTs), membrane-spanning bacterial lipids  
78 (Damsté et al., 2000). Several calibration studies in different settings (i.e. soils and lakes) have shown a correlation



79 between brGDGT abundances and mean annual air temperature (MAT) (e.g. De Jonge et al., 2014; Dearing Crampton-  
80 Flood et al., 2020; Russell et al., 2018; Weijers et al., 2007). These calibrations have been successfully used to  
81 quantitatively reconstruct continental temperature in marine river outflow and lacustrine sediments and terrestrial  
82 archives such as loess sequences and paleosoils (Loomis et al., 2015, 2017; Morrissey et al., 2018; Schreuder et al.,  
83 2016; Zeng and Yang, 2019; Garelick et al., 2022). Recently, global calibrations have been developed that suit cooler  
84 high-latitude lakes better (Martínez-Sosa et al., 2021; Raberg et al., 2021).

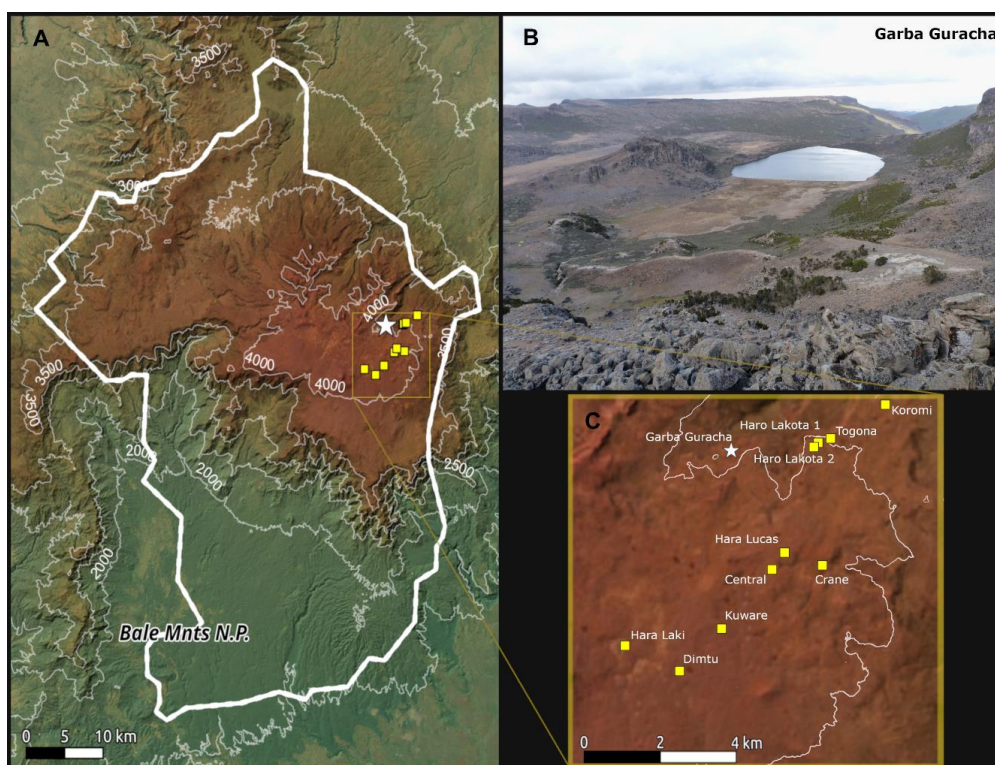
85 The phylogenetic breadth of the brGDGT-producing bacteria is still poorly constrained, although members from the  
86 phylum Acidobacteria have been proposed to produce brGDGTs both in cultures and in the environment (Sinninghe  
87 Damsté et al., 2018; De Jonge et al., 2019, 2021). Originally, Weijers et al. (2007b) found that the methylation (MBT)  
88 and cyclization of branched tetraethers (CBT) correlate with the measured mean annual air temperature (MAT) and  
89 pH values. Following the analytical separation of 5 and 6 methyl isomers, De Jonge et al. (2014) developed a new  
90 modified MBT'<sub>5ME</sub> ratio. This resulted in a revised calibration that removed the pH dependence affecting the  
91 MBT/MAT correlation and improved the accuracy of MAT reconstructions in terrestrial/soil archives. As brGDGT  
92 distributions recovered from lake sediments showed a different MAT dependence compared to soils, Russell et al.  
93 (2018) developed a MBT'<sub>5ME</sub> temperature calibration for lake sediments in eastern Africa. However, compared to the  
94 dataset of Russell et al. (2018), the brGDGT distribution of some Bale Mountain lake surface sediments are unique  
95 (Baxter et al., 2019). Although the MBT'<sub>5ME</sub> calibration by Russell et al. (2018) is a valuable supra-regional metric for  
96 reconstructing lake temperature, an adjusted calibration might better account for local conditions in the Bale region.

97 In this study, we aim to (i) compare brGDGT distributions from lake surface sediments of the Bale Mountains (n=11)  
98 (Baxter et al., 2019) with the eastern African dataset (Russell et al., 2018), (ii) develop a new ratio that captures the  
99 unique variation in the Bale Mountains and compare the accuracy of this calibrated ratio with the MBT'<sub>5ME</sub>, and (iii)  
100 reconstruct the first Horn of Africa high altitude paleotemperature record in the Bale Mountains using the sedimentary  
101 record of Garba Guracha (3950 m a.s.l.) and (iv) compare this Garba Guracha temperature record with other records  
102 in the region.



103 **2. REGIONAL SETTINGS**

104 **2.1 Study area**



105  
106 Figure 1: Location of the study area. (A) Bale Mountain National Park (thick white line), (B) a northeastward view over the glacial cirque of the  
107 Garba Guracha catchment (Bittner et al., 2021), and (C) Bale Mountain lakes in the dataset (yellow) - The map was created by the authors using  
108 QGIS 3.24 Tisler. All map layers are CC-by-SA v4.0, Image is from Bing Image / DigitalGlobe © Microsoft, DEM is from NASA/JPL SRTM  
109 (<http://www.jpl.nasa.gov/srtm/>) and the Bale Mountains National Park boundaries are from © OpenStreetMap contributors 2019. Distributed under  
110 the Open Data Commons Open Database License (ODbL) v1.0.

111

112 Garba Guracha (6.875781N, 39.878075E; Fig. 1) and all other lakes in this study are located east of the Main Ethiopian  
113 Rift in the Bale Mountains of the Bale-Arsi Massif. More specifically, they are situated on the Sanetti Plateau, the  
114 highest plateau in the Bale Mountains, between ~3800 to ~4200 m.a.s.l. and an area of 600 km<sup>2</sup> (Osmaston et al.,  
115 2005). Solidified horizontal lava consisting of tuffs with rhyolites, alkali basalt, and trachyte formed the volcanic  
116 plateau (Uhlig and Uhlig, 1991; Williams, 2016). The plateau and the valleys were partially glaciated at the Last  
117 Glacial Maximum (Groos et al., 2021, 2020; Osmaston et al., 2005; Ossendorf et al., 2019). The glacial cirque Garba



118 Guracha was first mentioned by Werdecker (1962) and was also described in depth by Umer et al. (2007) and Tiercelin  
119 et al. (2008). With a maximum water depth of 6 m and a very small catchment area, the lake is located at 3950 m above  
120 sea level. (0.15 km<sup>2</sup>; Fig. 1). The bedrock of the catchment is carbonate-poor (Löffler, 1978; Uhlig and Uhlig, 1991).  
121 An outlet towards the Togona Valley is present during the rainy season at the lake's northern end. A swampy alluvial  
122 plain fed by multiple springs stretches along the lake's southern shore.

123

## 124 **2.2 Climate**

125 The climate of the Bale Mountains varies spatially and temporally, affected by the orographic differences in altitude,  
126 a north-south exposure and by changing atmospheric air mass movements over the course of the year (Kidane et al.,  
127 2012; Uhlig and Uhlig, 1991). The Bale Mountains experience a four-month dry season (November to February) and  
128 a long wet season with complex orographic rainfall patterns (March to October) (Woldu et al., 1989; Kidane et al.,  
129 2012). The complexity of the rainfall pattern is associated with the convergence of northeast and southwest winds due  
130 to the northern and southern location of the ITCZ between June and September and between October and March,  
131 respectively (Tiercelin et al., 2008; Kidane et al., 2012). The Equatorial Westerlies and the Indian Ocean monsoon act  
132 as two moisture sources for the precipitation in the Bale Mountains (Miehe and Miehe, 1994; Uhlig, 1988). With 1000-  
133 1500 mm per year, the southern part of Bale Mountain experiences the highest precipitation amount, whereas the  
134 northern region, including Garba Guracha, only receives 800-1000 mm (Woldu et al., 1989). Temperatures vary  
135 seasonally, with the lowest temperatures in the dry season and the highest temperatures in the rainy season (Hillman,  
136 1988). The Afro-Alpine regions, including the Sanetti Plateau, are characterized by diurnal temperature differences  
137 between day and night (-15 to +26°C) (Hillman, 1988). Across the Bale Mountains, climate data has been collected  
138 since 2017 with a mean annual temperature of 4.9 °C (max. 6°C; min. 3.4 °C) at the Angesso Station, located at the  
139 same altitude 4 km northeast of Garba Guracha. The mean annual temperature at Garba Guracha is 5.4°C (Baxter et  
140 al., 2019).

141



142 **3. MATERIAL AND METHODS**

143 **3.1. Material and Sampling**

144 In this study, we used the data of 76 surface sediment samples from eastern African lakes. These lake sediments,  
145 located mainly in Ethiopia, Uganda and Kenya, were analyzed, and the results were published by Loomis et al. (2014,  
146 2011, 2012), Russell et al. (2018), Eggermont et al. (2011) and Baxter et al. (2019). The environmental data for the 11  
147 lakes in the Bale Mountains were published by Eggermont et al. (2011) and Baxter et al. (2019), and the corresponding  
148 MAT is based on a calculated lapse rate supported by local climate station data (Loomis et al., 2012; Russell et al.,  
149 2018).

150 At the Garba Guracha site, two overlapping sediment cores were retrieved in February 2017, at a water depth of 4.8 m  
151 using a Livingstone piston corer. A maximum sediment depth of 1550 cm was reached, covering an organic matter-  
152 rich upper section (0-900 cm) and an organic matter-poor bottom one (900-1550 cm). This study focuses on the last  
153 12.3 cal ka BP covering the 0-950 cm, with a mean sedimentation rate of 15 years/cm (more details on sediment  
154 properties and chronology can be found in Bittner et al. (2020)). We sampled at contiguous 10 cm intervals (average  
155 ~100 years of sedimentation). Thirty-five samples were selected for brGDGT analyses.

156 **3.2 Sample preparation and analysis**

157 The total lipid extracts (TLE) of the surface sediment samples were extracted using an accelerated solvent extractor  
158 (ASE) with dichloromethane:methanol in a ratio of 9:1 (Loomis et al., 2012). The brGDGTs were purified and  
159 separated according to their polarity. The samples were quantified following the method described by Huguet et al.  
160 (2006).

161 The TLE of the downcore sediments was obtained using a soxhlet system by constant rinsing (24h) with solvent  
162 (dichloromethane:methanol in a ratio of 9:1). After rotary evaporation, the TLE was redissolved in *n*-hexane and  
163 transferred onto a pipette column filled with aminopropyl silica gel (Supelco, 45 µm). Solvents of increasing polarity  
164 (*n*-hexane, dichloromethane/methanol 2:1; diethyl ether/acetic acid 19:1) were used to selectively elute the fractions  
165 of the TLE (nonpolar fraction A; two polar fractions B and C, including brGDGTs). Fraction B contained 98-99%,  
166 while fraction C contained 1-2% of all brGDGTs. All results refer to the brGDGTs contained in fraction B. Before  
167 measurement, a C<sub>46</sub> brGDGT standard was added, and the extract dried, redissolved in *n*-hexane/isopropanol (99:1)  
168 and filtered using a 0.45 µm polytetrafluoroethylene (PTFE) filter. The measurements of the GDGTs (dissolved in *n*-



169 hexane/IPA (99:1)) were done at ETH Zurich using a high-performance liquid chromatograph (Agilent 1260) coupled  
170 to a quadrupole mass spectrometer configured for atmospheric pressure chemical ionization (HPLC-APCI-MS). The  
171 separation of the GDGTs was achieved by two silica columns at 45°C (modified after Hopmans et al. (2016)) with a  
172 flow rate of 0.2ml/min and an injection volume of 10 µl. Compound-peak integrations of  $m/z$  1292, 1050, 1048, 1046,  
173 1046, 1034, 1032, 1022, 1020, 1018 and 744 were performed according to previously published methods (Hopmans  
174 et al., 2016).

### 175 3.3 BrGDGTs – structure, statistical methods and proxy calculation

176 BrGDGTs can be present as tetra- (I), penta- (II), or hexamethylated compounds with different numbers of cyclopentyl  
177 moieties (none (a), one (b), or two (c)). The outer methyl group can be positioned on the  $\alpha$  and/or C5 (5-methyl  
178 compounds) or C6 (6-methyl compounds, indicated by a prime notation) location (De Jonge et al., 2014). To interpret  
179 the GDGT composition of the samples, we used the BIT, MBT', MBT'<sub>SME</sub>, and CBT' (Table 1).

180 We calculated the BIT index following the equation of Hopmans et al. (2004):

$$181 \text{ BIT index} = (Ia + IIa + IIIa + IIa' + IIIa') / (Ia + IIa + IIIa + IIa' + IIIa' + \text{crenarchaeol}) \quad [\text{Eq. 1}]$$

182 De Jonge et al. (2014) showed that the MBT' ratio (Peterse et al., 2012) contains 5- and 6-methyl compounds that are  
183 explicitly mentioned here:

$$184 \text{ MBT}' = (Ia + Ib + Ic) / (Ia + Ib + Ic + IIa + IIa' + IIb + IIb' + IIc + IIc' + IIIa + IIIa') \quad [\text{Eq. 2}]$$

185 By removing the 6 methyl isomers from the equation, De Jonge et al. (2014) improved the temperature calibration  
186 further:

$$187 \text{ MBT}'_{\text{SME}} = (Ia + Ib + Ic) / (Ia + Ib + Ic + IIa + IIb + IIc + IIIa) \quad [\text{Eq. 3}]$$

188 The cyclization of branched tetraethers (CBT') is calculated following the equation from De Jonge et al. (2014a):

$$189 \text{ CBT}' = {}^{10}\log (Ic + IIa' + IIb' + IIc' + IIIa' + IIIb' + IIIc') / (Ia + IIa + IIIa) \quad [\text{Eq. 4}]$$

190 The fractional abundance of any individual brGDGT compound (i) was defined as:

$$191 f(i) = i / (Ia + Ib + Ic + IIa + IIa' + IIb + IIb' + IIc + IIc' + IIIa + IIIa' + IIIb + IIIb' + IIIc + IIIc') \quad [\text{Eq. 5}]$$

192



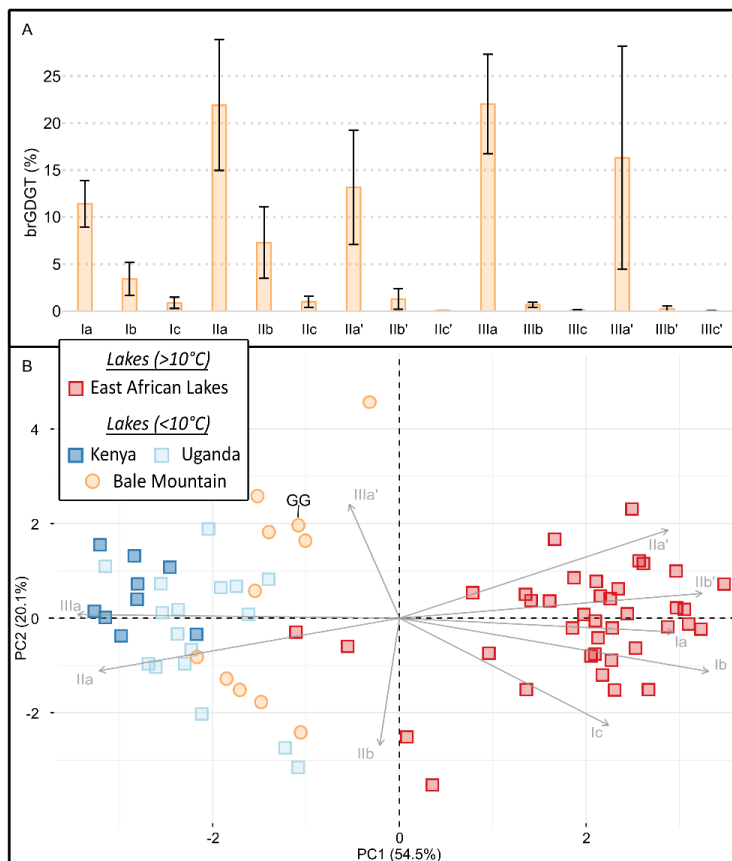
193 **3.4 Quantitative data analyses**

194 Numerical analyses in this paper have been performed with Excel and R 4.1.0 (R Core Team, 2021). Results are  
195 displayed using the arithmetic mean and standard deviations using the notation  $\pm$ . To explore the correlation level  
196 between brGDGTs and MAT, we used linear regressions and the reported Pearson correlation values ( $r^2$ ), where  
197 significant correlations were considered when the p-value  $< 0.05$ . We performed a Principal Component Analysis  
198 (PCA) of brGDGTs from i) the calibration dataset and ii) the Garba Guracha record, based on standardized and scaled  
199 fractional abundance. The ordination methods provide a simple yet effective way to visualize the variability within the  
200 distribution of the brGDGTs. PCA was performed with the R package *factoextra* (Kassambara and Mundt, 2020).



201 **4. RESULTS**

202 **4.1 BrGDGT patterns of surface sediments from lakes in the Bale Mountains**



203

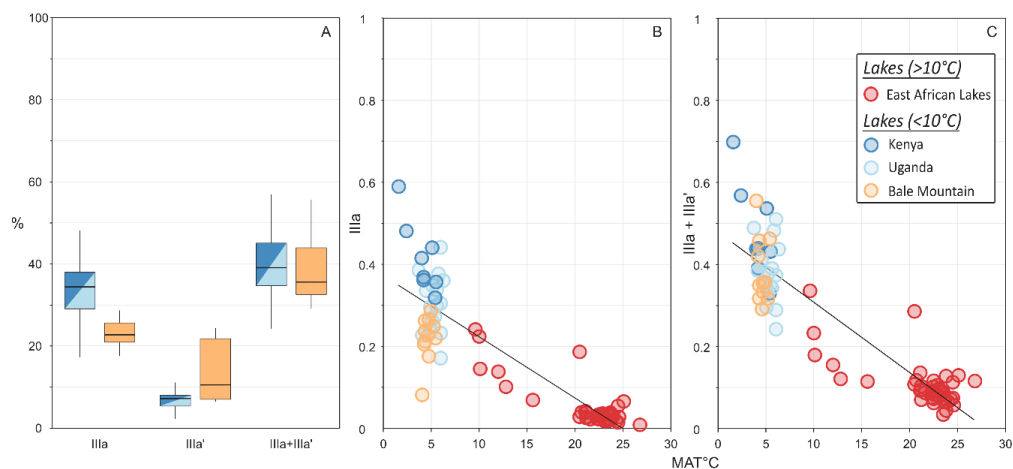
204 Figure 2: (A) Barplot of average brGDGT percentages in Bale Mountain lake surface sediments (Baxter et al., 2019), with standard deviation plotted  
205 as error flags and (B) PCA of brGDGTs of eastern African lakes with regional pattern; data from Russell et al. (2018) and Baxter et al. (2019) -  
206 lakes >10°C (purple) and lakes <10°C (red, turquoise and green); Garba Guracha (GG).

207

208 To frame the downcore variation in Garba Guracha in the current environmental settings, we have expanded the dataset  
209 of Russel et al. (2018) by 11 Bale Mountain lake surface sediment samples (Table S1 and S2) (data from Baxter et al.,  
210 2019). Due to the missing values of IIc, IIc', IIIb, IIIb', IIIc and IIIc' in the dataset of Russell et al. (2018), we excluded  
211 these isomers in the Bale Mountain data from the PCA to compare the datasets (see the supplementary Figure S1 for a  
212 PCA including all isomers). The highest fractional abundances of brGDGTs in these surface sediments are (i) IIIa with  
213 a mean of 22% ( $\pm 5$ ), (ii) IIa with a mean of 22% ( $\pm 7$ ) and (iii) IIIa' with a mean of 16% ( $\pm 12$ ) (Fig. 2A, Table S2).



214 The PCA of brGDGTs shows some differences between the East African lake dataset and the Bale Mountain lakes  
215 (Fig. 2B). IIIa and IIa have negative loadings, and IIa', IIB', Ia, Ib and Ic have positive loading on PC1. PC2 has negative  
216 loadings from IIB and positive loading from IIIa' and IIa'. The Bale Mountain lakes have a negative score on PC1,  
217 consistent with their location in a cool climate. At the same time, the Bale Mountain lakes have a wider dispersion on  
218 PC2 than the East African lake dataset. On PC2, a decrease of 5ME cyclopentane of brGDGTs IIB and an increase of  
219 6 ME brGDGT IIIa' is visible in some of the Bale Mountain lakes, including Garba Guracha.  
220 Compared to similar high altitude lakes (above 3500 m) in eastern Africa (East African lake dataset (Russell et al.,  
221 2018)), the percentage of IIIa and IIa is lower, and the IIIa' and IIa' is higher in the Bale Mountain lakes (Fig 3).  
222 Interestingly, the combined percentage of these 5 and 6 methyl isomers is similar (Fig. 3 A).  
223



224  
225 Figure 3: (A) Abundance of IIIa and IIIa' in percent; (B) Linear correlation between IIIa and MAT ( $r^2 = 0.78$ ) and (C) IIIa + IIIa' to MAT ( $r^2 = 0.82$ )  
226 - data from Russell et al. (2018) - lakes  $>10^\circ\text{C}$  (purple) and lakes  $<10^\circ\text{C}$  (red and green); Bale Mountain lakes (Baxter et al., 2019) (turquoise).  
227

228 We hypothesize that the 6-methyl compound (IIa' and IIIa') is produced instead of their 5-methyl counterparts (IIa and  
229 IIIa) in some of the Bale Mountain lakes. Moreover, in the East African lake dataset, the correlation of IIIa to MAT  
230 ( $r^2 = 0.78$ ) is slightly improved by adding IIIa' to  $r^2 = 0.82$  (Fig 3 B and C). Although the production of IIIa' at the  
231 expense of IIIa is poorly understood in lacustrine settings, it clearly has the potential to influence MBT'<sub>5ME</sub> values.  
232 Indeed, MBT'<sub>5ME</sub> values of the Bale Mountain lakes range from 0.20 to 0.37, with a mean of 0.24 ( $\pm 0.05$ ). As the MAT  
233 range of Bale Mountain lakes is limited (4-5.4 °C), the range of MBT'<sub>5ME</sub> is larger than expected of the measured MAT



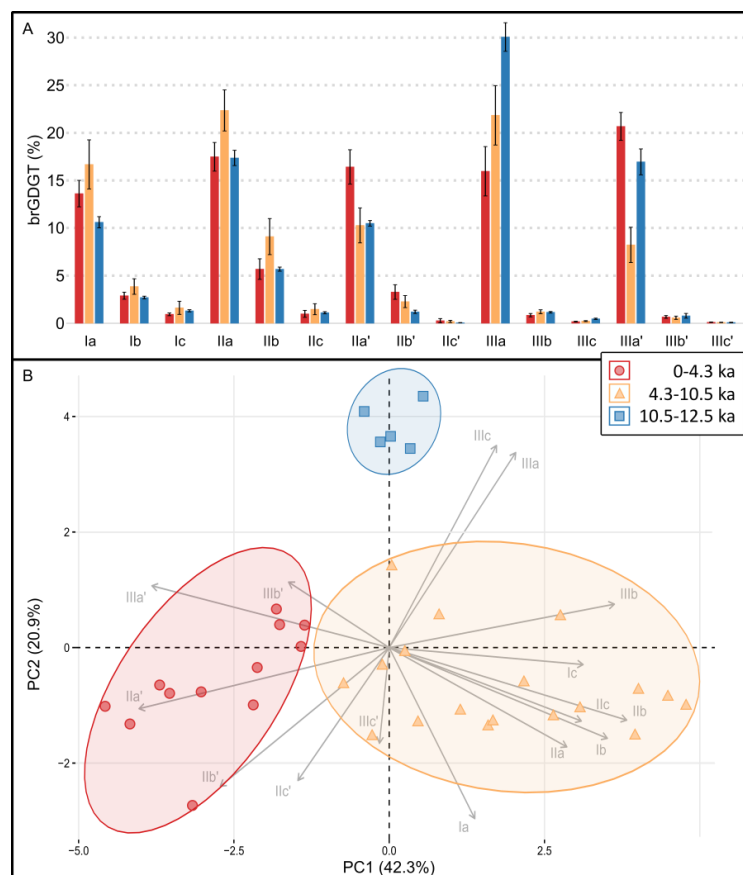
234 relative to similar eastern African lakes in the East African lake dataset ( $MBT'_{5ME} = 0.17$  to  $0.25$  with a mean of  $0.22$   
235  $\pm 0.02$ ;  $MAT = 4-5.4$  °C) (Russell et al., 2018). Moreover, regional variations in brGDGT isomers, especially in Bale  
236 Mountain surface sediments, appear in the degree of cyclization (DC') and CBT' in the eastern African lake surface  
237 sediment data (Russell et al., 2018; Baxter et al., 2019) (Fig. S2).

#### 238 **4.2 BrGDGT patterns of the Garba Guracha sediment core**

239 In the Garba Guracha sediments, both branched and isoprenoid GDGTs are present. The BIT index ranges between  
240  $0.8$  and  $1$  (mean= $0.98$ ,  $\pm 0.04$ ). Only the oldest samples ( $12-10$  cal ka BP) have a lower BIT index value of  $0.8$  to  $0.9$   
241 (Table S3). Tetramethylated brGDGTs in the sediment core represent on average  $19.5\%$ , pentamethylated brGDGTs  
242  $44\%$ , and hexamethylated brGDGTs  $36.5\%$  (Table S3). The highest fractional abundances are (i) IIIa with a mean of  
243  $21\%$  ( $\pm 5$ ), (ii) IIa with a mean of  $20\%$  ( $\pm 3$ ) and (iii) Ia with a mean of  $15\%$  ( $\pm 3$ ). The  $MBT'_{5ME}$  ranges from  $0.20$  to  
244  $0.35$  with a mean of  $0.28$  ( $\pm 0.04$ ) (Table S4). The CBT' ratio ranges from  $0.06$  to  $-0.54$  with a mean of  $0.27$  ( $\pm 0.18$ )  
245 (Table S3).

246 A PCA of all downcore brGDGTs distributions (Fig. 4A) shows that the first two components explain  $63.2\%$  of the  
247 variance. On PC1 ( $42.3\%$ ), all 6 methyl isomers have negative loadings, while 5 methyl isomers show positive  
248 loadings. PC2 ( $20.9\%$ ) shows positive loadings of all hexamethylated brGDGTs and negative loadings of all penta-  
249 and tetramethylated brGDGTs. The PCA reveals changes in brGDGT composition with core depth when the data  
250 points are grouped using the following age cut-offs: ( $0-4.3$  cal ka BP;  $4.3-10.5$  cal ka BP;  $10.5-12.5$  cal ka BP) (Fig.  
251 4A). In phase 1 ( $12.5 - 10.5$  cal ka BP), IIIa, IIIa' and IIa have the highest mean abundances of  $30\%$ ,  $17\%$ , and  $17\%$ ,  
252 respectively. In phase 2 ( $10.5 - 4.3$  cal ka BP), the mean abundance of IIIa and IIIa' are decreased by around  $9\%$ , while  
253 IIa, IIb and Ia increase. In phase 3 ( $4.3 - 0$  cal ka BP), the mean abundances of IIIa decrease by  $6\%$  further. Conversely,  
254 the mean abundance of IIIa' increases again by  $12\%$ . The same holds true for IIa ( $-5\%$ ) and IIa' ( $+6\%$ ). The mean  
255 abundance of Ia increases further by  $3\%$  (Fig 4B).

256



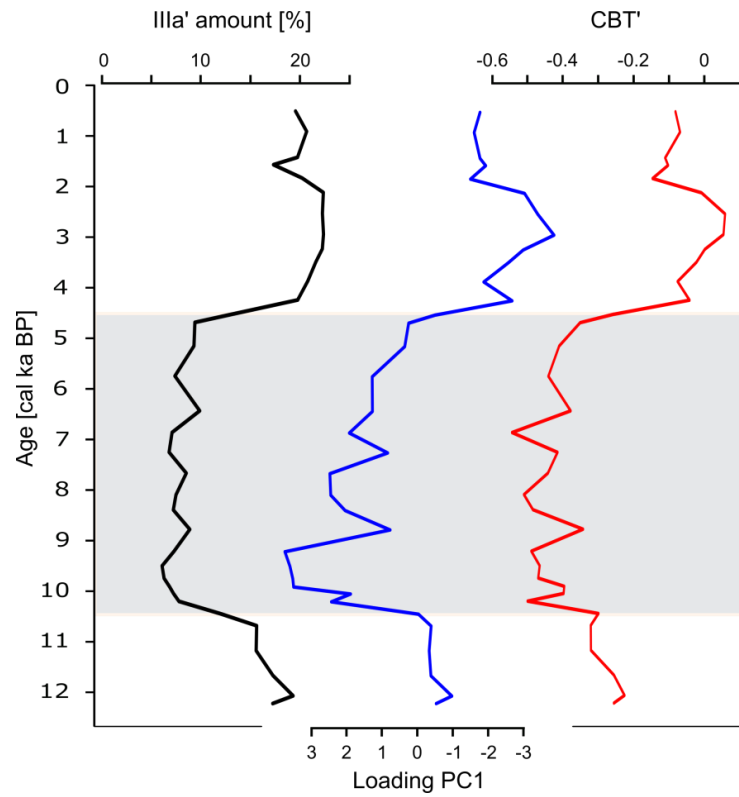
257

258 Figure 4: (A) PCA of brGDGTs of the Garba Guracha sediment core; data from 0 to 4.3 cal ka BP (red), data from 4.3 to 10.5 cal ka BP (orange)  
259 and data from 10.5 to 12.5 cal ka BP (blue); (B) barplot of average brGDGT percentages in the Garba Guracha sediment core, with standard deviation  
260 plotted as error flags.

261

262 The unusually high abundance of brGDGTs IIIa' compared to IIIa observed in surface sediments of Bale Mountains  
263 lakes (Fig. 2A) is also visible in the Garba Guracha record. The relative abundance of IIIa' varies with depth. High  
264 amounts of IIIa' appear until 10.8 cal ka BP followed by low percentage (<10%) until 4.5 cal ka BP. The highest  
265 abundance of IIIa' with up to 22% occurs after 4.5 cal ka BP until the recent past. The changing abundances of IIIa' in  
266 our record coincide with changes in CBT' (Fig. 5). The variability in the 6-methyl brGDGTs reflects the largest part  
267 of the variation in this dataset, reflected by the good agreement ( $r^2= 0.77$ ,  $p<0.001$ ) between the fractional abundance  
268 of brGDGTs IIIa' and the sample loadings on PC1.

269



270

271 Figure 5: Downcore functions for Illal amount, the PC1 loading and CBT' of the Garba Guracha brGDGT record.

272



273 **5. DISCUSSION**

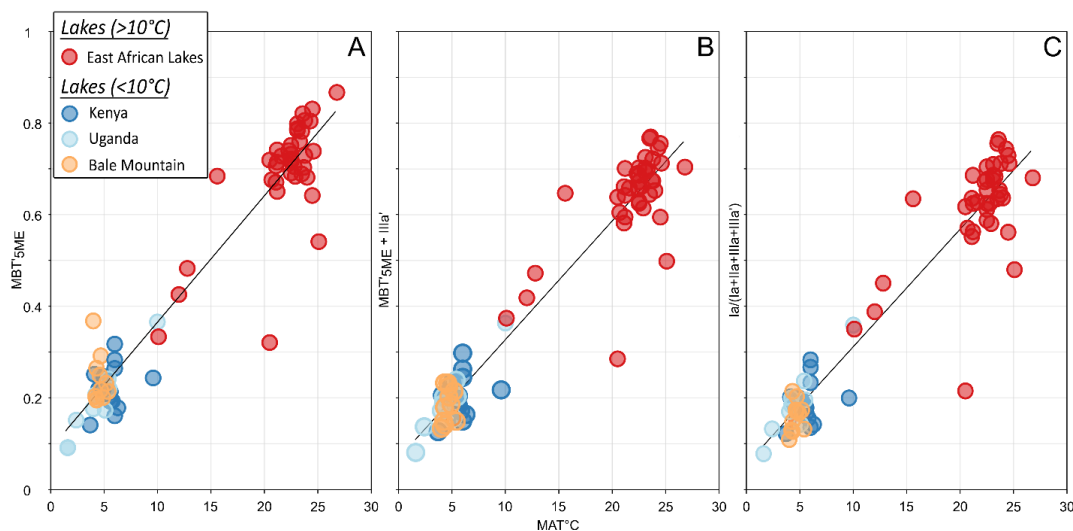
274 **5.1 Possible MAT calibration functions inferred from the expanded east African surface sediment dataset**

275 *Table 1: Temperature calibrations – Ratios, calibration dataset,  $r^2$ , and root-mean-square-error (RMSE) in °C*

Ratio		Calibration dataset	$r^2$	RMSE °C
MBT' <sub>SME</sub> (Ia+Ib+Ic)/(Ia+Ib+Ic+IIa+IIb+IIc+IIIa)		EAL (n=65)	0.92	2.41
		EAL <sub>BM</sub> (n=76)	0.92	2.41
MBT' <sub>SME</sub> + IIIa' (Ia+Ib+Ic)/(Ia+Ib+Ic+IIa+IIb+IIc+IIIa+IIIa')	[Eq. 6]	EAL <sub>BM</sub> (n=76)	0.93	2.38
MBT' <sub>SME</sub> + IIa'&IIIa' Ia/(Ia+IIa+IIIa+IIa'+IIIa')	[Eq. 7]	EAL <sub>BM</sub> (n=76)	0.84	3.48
Simplified MBT' <sub>SME</sub> + IIIa' Ia/(Ia+IIa+IIIa+IIIa')	[Eq. 8]	EAL <sub>BM</sub> (n=76)	0.91	2.59

276  
 277 We added the GDGT distribution data of 11 surface sediments from Bale Mountains lakes (Baxter et al., 2019) to the  
 278 existing data of Russell et al. (2018) and applied the MBT'<sub>SME</sub> calibration (Table 1). Here, the original dataset (n = 65)  
 279 is referred to as East African Lakes "EAL", while the extended dataset (n = 76) is referred to as East African Lakes +  
 280 Bale Mountain lakes (EAL<sub>BM</sub>). The linear correlation between the MBT'<sub>SME</sub> and MAT was almost identical after adding  
 281 the 11 Bale Mountain lake samples (EAL  $r^2=0.92$ , EAL<sub>BM</sub>  $r^2=0.93$ ). To test whether the unique brGDGT distribution  
 282 in some Bale Mountain lakes (Fig. 2) affected the temperature correlation, we applied various calibrations to account  
 283 for the increased abundance of IIIa' (and to a lesser extent IIa'). Including these compounds is *a priori* supported by  
 284 global scale calibrations, as Raberg et al. (2021) showed that a global temperature calibration with a modified MBT'  
 285 ratio that includes IIIa' and IIa' (Table 6, Eq. 7) correlates with month above freezing (MAF) in lakes ( $r^2=0.90$ , RMSE=  
 286 2.18) almost as well as the unmodified MBT'<sub>SME</sub> ratio. In the EAL<sub>BM</sub> dataset, the application of this ratio has a lower  
 287  $r^2$  of 0.84 and a higher RMSE of 3.48°C compared to the MBT'<sub>SME</sub> (Table 1: Eq. 7). As brGDGT IIIa' specifically was  
 288 shown to increase in Bale Mountain sediments and improved the correlation with MAT (Fig. 3B and C), we  
 289 investigated alternative ratios that incorporate this compound but exclude IIa'. Table 1 and Fig. 6 summarize the  
 290 correlation coefficients of the MBT'<sub>SME</sub> ( $r^2=0.92$ , RMSE of 2.41°C), an MBT'<sub>SME</sub> ratio that includes IIIa' (Eq. 6) with  
 291  $r^2=0.93$  and RMSE of 2.38°C and the simplified ratio that includes only the major brGDGTs compounds (Eq. 8:  $r^2=$   
 292 0.91 and an RMSE of 2.59°C).

293



294

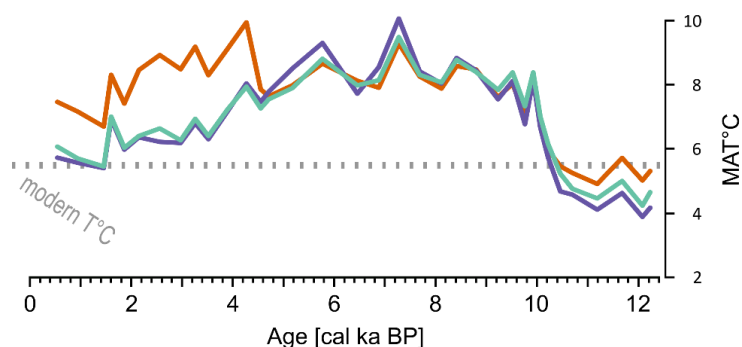
295 Figure 6: Correlations EAL<sub>BM</sub> datasets, (A)  $MBT'_{5ME}$  ( $r^2 = 0.92$ ; RMSE of 2.41); (B)  $MBT'_{5ME} + IIIa'$  ( $r^2 = 0.93$ ; RMSE of 2.38.); (C)  
 296  $Ia/(Ia+IIa+IIIa+IIIa')$  ( $r^2 = 0.91$ ; RMSE of 2.59) - data from Russell et al. (2018) - lakes  $>10^\circ C$  (purple) and lakes  $<10^\circ C$  (red and green); Bale  
 297 Mountain lakes (Baxter et al., 2019) (turquoise).

298 The results of  $Ia/(Ia+IIa+IIIa+IIIa')$  ( $MAT = -0.773 + 35.646 \times Ia/(Ia+IIa+IIIa+IIIa')$ ) and  $MBT'_{5ME} + IIIa'$  ( $MAT = -$   
 299  $1.4734 + 35.777 \times MBT'_{5ME} + IIIa'$ ) calibrations are very similar ( $r^2=0.97$ ) (Fig. 7, purple and green curves,  
 300 respectively). Therefore, we discuss only the best performing  $MBT'_{5ME}$  ( $MAT = -1.8299 + 33.304 \times MBT'_{5ME}$ ) and the  
 301  $MBT'_{5ME} + IIIa'$  calibration developed using the EAL<sub>BM</sub> dataset to the downcore distributions.

302

303 **5.2 Paleotemperature reconstructions for the Garba Guracha sedimentary record - comparison of the different**  
 304 **calibrations**

305



306

307 Figure 7: Reconstructed temperatures of the Garba Guracha sedimentary record.  $MBT'_{SME}$  (orange);  $Ia/(Ia+IIa+IIIa+IIIa')$  (purple);  $MBT'_{SME} + IIIa'$   
308 (turquoise).

309

310 We evaluate the downcore trend in GG sediments to compare the performance of both calibrations, revealing periods  
311 of agreement (10-4.2 ka BP) and a period of temperature offset (since 4.2 ka BP). Using established and newly  
312 developed ratios and calibrations (Russell et al., 2018; this paper) resulted in similar absolute values and comparable  
313 temperature trends, principally in the early and mid-Holocene. Reconstructed temperatures range from 4.9 to 10.0°C  
314 ( $MBT'_{SME}$ ) and 4.2 to 9.5°C ( $MBT'_{SME} + IIIa'$ ) (Fig. 7). Despite a slightly different range in temperature (4.4 and 5.3  
315 °C), the trends of both calibrations are similar between 12 and 4.7 cal ka BP. The lowest MATs (< 5°C) occurred  
316 between 12.2 cal ka BP (950 cm) and 10.5 cal ka BP (800 cm). MAT increased rapidly by 3.5°C between 10.5 cal ka  
317 BP (800 cm) and ca. 10 cal ka BP (700 cm). During the early to mid-Holocene, a thermal maximum occurred between  
318 10 and 5.7 cal ka BP (440 cm), with the highest MAT values reaching ca. 10°C.

319 At ~6.5 cal ka BP, the MAT decreased for both calibrations. The temperature drop coincides with organic-poor layers  
320 in the sediment core formed during a drought, concurring with low monsoonal intensity (Bittner et al., 2020). While  
321 drought phases are not directly linked to changing temperatures, in the monsoonal systems of eastern Africa,  
322 temperature and precipitation seem to be more connected (Costa et al., 2014; Loomis et al., 2015).

323 A strong offset between the calibrations appeared at 4.2 cal ka BP. Using the  $MBT'_{SME}$ , we reconstruct a sudden  
324 temperature rise (Fig. 7) that contrasts with the temperature decrease when using the  $MBT'_{SME} + IIIa'$  calibration at a  
325 moment when temperatures are expected to decrease in phase with insolation (Fig. 7). The offset coincides with a  
326 known drought phase and is accompanied by shifts of many proxies (TOC,  $\delta^{13}C$ , TOC/N, *Erica spp.*, charcoal) in the



327 Garba Guracha record (Bittner et al., 2020; Gil-Romera et al., 2019). The changing conditions in the Garba Guracha  
328 catchment during this drought phase, especially the decline of the *Erica* shrubland (Gil-Romera et al., 2019), could  
329 have resulted in an increase in the lake water pH. A change in the lake water chemistry is supported by a decrease in  
330 CBT' ratio (Fig. 5). In lakes on a global scale, CBT' correlates with pH and conductivity (Raberg et al., 2021). In the  
331 last years, studies have suggested that the change in brGDGT composition captured by the CBT' may change due to  
332 shifting bacterial communities in soils and lakes (De Jonge et al., 2019; van Bree et al., 2020; Weber et al., 2018).  
333 Previously, pH-dependent community changes have been shown to affect MBT'<sub>5ME</sub> values in soils (De Jonge et al.,  
334 2021), and we propose that a similar effect can be seen in Garba Guracha.

335 Hence we suggest that MBT'<sub>5ME</sub> systematically overestimates the temperatures of Garba Guracha during the late  
336 Holocene after 4 cal ka BP. A systematic offset is further supported by continuously and similarly decreasing  
337 reconstructed temperatures using both calibrations until the top of the core with a shared maximum at 150 cm (1.6 cal  
338 ka BP). We suggest that the production of IIIa' at the expense of IIIa is increased during dryer intervals, possibly caused  
339 by a change in lake water chemistry and/or bacterial communities. We conclude that a temperature calibration  
340 including IIIa' allows to reconstruct MAT in Garba Guracha sediments more accurately, as it accounts for the unique  
341 and variable production of IIIa' in Bale Mountain lakes.

### 342 **5.3 Paleotemperature reconstructions for the Garba Guracha sedimentary record – regional comparison**

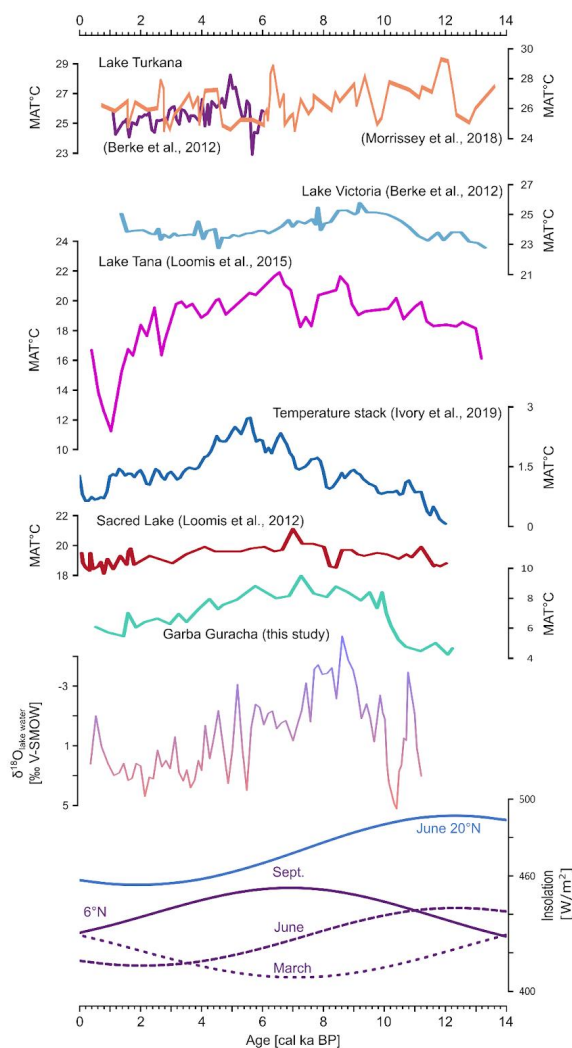
#### 343 5.3.1. Deglacial warming

344 Overall, the recorded temperature trends in Garba Guracha are in phase with northern summer insolation variability  
345 (Fig. 8). This is reasonable because air temperature and insolation are closely connected (Huybers, 2006). However,  
346 the coldest MATs (<5°C) were recorded before 10.5 cal ka BP even though the northern hemisphere summer (20°N)  
347 insolation maxima occurred already 12 cal ka BP (Fig. 8). Tiercelin et al. (2008) argue that in Garba Guracha, ice  
348 remained in the catchment until ~10 cal ka BP due to topographical conditions, especially the north-facing exposition  
349 of the valley. The remaining ice in the basin might have (i) reduced the temperature of the lake water by inflow of cold  
350 melt water and (ii) buffered the warming caused by increasing insolation. Indeed, rising temperatures were recorded  
351 in other eastern African records as early as 14 cal ka BP (Lake Tana) (Loomis et al., 2015; Tierney et al., 2016).

352 Similar to Lake Tana, but ~4000 years later, MAT (°C) in the Garba Guracha record experienced an abrupt increase  
353 of ca. 3.5°C in just ca. 600 years, from 10.5 to 9.9 cal ka BP. Simultaneously with the rise in temperature, Bittner et



354 al. (2021) found an increase in P/E, indicating higher moisture availability based on depleting values of reconstructed  
355  $\delta^{18}\text{O}_{\text{lake water}}$ . At Lake Tana, Loomis et al. (2015) and Costa et al. (2014) attribute a similar connection between warmer  
356 temperature and depleted water isotopes ( $\delta^2\text{H}$ ) since 13.8 cal ka BP to the penetration of warm Congo Basin air masses  
357 resulting in weaker easterly trade winds and a strengthening of the southwesterly winds and the Somali Jet. The con-  
358 nection between Congo Basin air masses and eastern Africa is supported by the absence of cold temperatures associated  
359 with the Younger Dryas (YD) in both the Congo Basin temperature record (Weijers et al., 2007a) and Lake Tana  
360 (Loomis et al., 2015). However, in the Garba Guracha record, lower temperatures prevailed 4000 years longer than in  
361 Lake Tana (Loomis et al., 2015). Although catchment glaciers could have caused these conditions in Garba Guracha,  
362 the low temperatures are accompanied by a reduced sedimentation rate between 12.8 and 11.3 cal ka BP (Bittner et al.,  
363 2020), pointing to climatic influences associated with YD times (Alley, 2000). Indeed, other records from the Horn of  
364 Africa indicate dry conditions associated with the YD period, like Lake Ashenge (Marshall et al., 2009) and the marine  
365 record of the Gulf of Aden (Tierney and deMenocal, 2013). Therefore, we suggest that, at least for some periods, the  
366 climate drivers operating in the Garba Guracha region might have been different from other parts of eastern Africa.  
367 The time lag between Lake Tana and Garba Guracha could be explained by a slow eastwards advance of the Congo  
368 Air Boundary and different climatic conditions at the sites. However, with the current data, we are unable to precisely  
369 distinguish between north hemisphere YD forcing, remaining ice in the lake catchment, or regional atmospheric cir-  
370 culation change affecting the Garba Guracha record.



371

372 Figure 8: Comparison of records. MAT: Lake Turkana (Berke et al., 2012; Morrissey et al., 2018); Lake Victoria (Berke et al., 2012); Lake Tana  
373 (Loomis et al., 2015); eastern Africa temperature stack (Ivory et al., 2019); Sacred Lake (Loomis et al., 2012); Garba Guracha (this study);  $\delta^{18}\text{O}_{\text{lake water}}$   
374 as reconstructed from the aquatic sugar biomarker fucose (Bittner et al., 2021) and insolation 6°N and June 20°N (Laskar et al., 2004).

### 375 5.3.2. Warm temperatures during the African Humid Period in eastern Africa

376 Regardless of the cause, the ~10.5 cal ka BP rise in MAT is associated with an abrupt increasing moisture availability  
377 and changes of vegetation around Garba Guracha (Gil-Romera et al., 2021; Umer et al., 2007). Vegetation and fire  
378 dynamics around Garba Guracha responded dynamically to the changing climatic conditions, evidencing the sensitivity



379 of the afroalpine plant communities to increasing temperature. As MAT increased between 11 and 10 cal  
380 ka BP, the ericaceous belt expanded (Gil-Romera et al., 2021). The rising temperature and increasing P/E (Bittner et  
381 al., 2021) were accompanied by the expansion of the afroalpine vegetation cover (Gil-Romera et al., 2021; Miede and  
382 Miede, 1994). An immediate consequence of the temperature rise and increasing moisture availability was biomass  
383 accumulation, as evidenced by the change from organic matter-poor to organic matter-rich sedimentation (Bittner et  
384 al., 2020) and the expansion of heathlands (Gil-Romera et al., 2019). Under an increasing MAT and extending biomass,  
385 fire activity was very intense at this time (Gil-Romera et al., 2019).

386 The thermal maximum of the Garba Guracha record spanned from 9 to 5.8 cal ka BP, with the highest reconstructed  
387 temperatures occurring at 7 cal ka BP. A similar mid-Holocene thermal optimum has been recorded at Sacred Lake (7  
388 cal ka BP) and Lake Tana (7 cal ka BP) (Fig 8). However, the highest temperatures of Lake Victoria occurred at 9 cal  
389 ka BP, and of Lake Rutundu, Lake Malawi and Lake Tanganyika at 5 cal ka BP (Berke et al., 2012b; Loomis et al.,  
390 2017, 2015, 2012; Powers et al., 2005; Tierney et al., 2008). At Lake Turkana, the thermal optimum occurred at 6.4  
391 cal ka BP (Morrissey et al., 2018) or 5 cal ka BP (Berke et al., 2012a). A new temperature reconstruction from Lake  
392 Mahoma (Garellick et al., 2022) and a temperature stack including temperature reconstructions from Sacred Lake, Lake  
393 Malawi, Lake Tanganyika, Lake Rutundu, and the Congo Basin by Ivory and Russell (2018) showed the highest tem-  
394 peratures between ~7 and ~4.5 cal ka BP. The timing of the highest reconstructed temperatures at these sites is not  
395 related to greenhouse gas radiative forcing or insolation forcing (Loomis et al., 2015). Loomis et al. (2015) point out  
396 that the Lake Tana and Sacred Lake temperature maxima lag northern hemisphere summer insolation, and Lake Ma-  
397 lawi and Lake Tanganyika lead peak southern summer insolation. In the case of Garba Guracha, the highest tempera-  
398 tures coincide with local maximum September insolation at the sites latitude of 6°N (Laskar et al., 2004) (Fig. 8). This  
399 matches the suggestion of Berke et al. (2012a) that the thermal optimum of several eastern African lakes might be  
400 determined by local solar irradiance from Sep to Dec (maximum at ~6 cal ka BP) (Fig. 8) rather than northern hemi-  
401 sphere summer solar irradiance. The restratification processes of eastern African lakes in these months and associated  
402 epilimnetic heating might explain the increased warming of lake water (Berke et al., 2012a). However, modelling  
403 studies do not support this hypothesis (Dee et al., 2021).

404 In addition to local insolation changes, local changes in P/E could have the potential to modify the lake water temper-  
405 ature. During the Early and Mid-Holocene, reconstructed high temperatures occurred during the African Humid Period,  
406 accompanied by the wettest phase of Garba Guracha (Bittner et al., 2021) and rising lake levels in the region (Gasse,



407 2000; Junginger et al., 2014), indicating higher amounts of precipitation due to an intensification of the monsoon  
408 system. A modelling study (Tierney et al., 2011b) proposes that during the AHP, the precipitation increase occurred  
409 mainly in June, July, and August (JJA), shortening the duration of annual drought phases in eastern Africa. Increased  
410 relative humidity would reduce evaporation, limiting the evaporative cooling of the lake water. Less evaporation, either  
411 due to shorter drought phases or generally higher precipitation, would increase the temperature and cause less positive  
412  $\delta^{18}\text{O}_{\text{lake water}}$  values, as suggested for Garba Guracha (Bittner et al., 2021).

413 The highest temperatures of the Holocene continued until 5.8 cal ka BP, interrupted only by a short drop in temperature  
414 after 7 cal ka BP. This is in agreement with the Sacred Lake temperature record (Loomis et al., 2012). Lake Tana  
415 experienced a shift towards colder conditions a bit earlier, from 7.5 to 7 cal ka BP (Loomis et al., 2015).

#### 416 5.3.3. cooling in the Late Holocene

417 After 5.8 cal ka BP, the MAT continuously decreased by  $\sim 3.6^\circ\text{C}$  until recent times, coinciding with the summer inso-  
418 lation decline and decreasing temperatures of equatorial lakes (Ivory and Russell, 2018), Lake Tana (Loomis et al.,  
419 2015) and the marine Gulf of Aden record (Tierney et al., 2016). The general decreasing temperature trend is also  
420 supported by  $\delta^{18}\text{O}_{\text{lake water}}$ , pollen and charcoal results showing a decrease in moisture availability and fire activity  
421 (Bittner et al., 2021; Gil-Romera et al., 2019). Furthermore, an upwards shift of the lower and dry forests during this  
422 time reinforces the idea of more intense evapotranspiration due to the decrease in moisture availability (Gil-Romera et  
423 al., 2021). A drop in TOC and decreasing  $\delta^{13}\text{C}$  values (Bittner et al., 2020) support overall shifting catchment condi-  
424 tions.

425 During the last two thousand years, we observed that the increasing temperature trend concurred with an abrupt in-  
426 crease in the main woody communities and enhanced fire activities around Garba Guracha (Gil-Romera et al., 2021).  
427 However, we cannot discard human influence favouring both woody encroachment and fire activity.

428 The strong connection of temperature, P/E and insolation across the Holocene shows that the Garba Guracha temper-  
429 atures might have been affected by local radiation, possibly in interplay with insolation-driven atmospheric circulation  
430 changes and their impacts on air mass source, cloud cover and evaporation. As current global warming continues, the  
431 intense warming of landmasses could lead to a major and complex restructuring of the atmospheric circulation system  
432 in the future, affecting eastern Africa and possibly even larger regions beyond via teleconnections.



433 **6. CONCLUSIONS**

434 The eastern African climatic history is spatially very diverse, and the driving mechanisms are complex and not fully  
435 understood. In eastern Africa, temperature reconstructions are generally sparse, especially in the high altitudes of the  
436 Horn of Africa. In this study, we used brGDGT from a high altitude sedimentary record of the Bale Mountains (lake  
437 Garba Guracha, Southwestern Ethiopia) to produce the first temperature reconstruction for the Horn of Africa.

438 The composition of brGDGT isomers in sediment records is affected by several influences, mainly by MAT, but in  
439 addition by lake water chemistry and bacterial community, resulting in locally unique brGDGT compositions. For  
440 instance, in some of the Bale Mountain lakes, the abundance of a specific isomer IIIa' is uncommonly high in surface  
441 sediments. However, the summed abundance of IIIa and IIIa' is similar to other comparable lake archives in eastern  
442 Africa. We suspect that in the case of the Bale Mountains, changes in the lake's water chemistry or bacterial community  
443 are responsible for the high production of IIIa' at the expense of IIIa under drier conditions. By including the 6 methyl  
444 isomer in a temperature calibration, we were able to enhance the correlation with MAT. Therefore, we conclude that  
445 6 methyl isomers have an impact on temperature reconstructions, highlighting their inclusion in a Bale Mountain-  
446 specific temperature calibration. Using surface sediment data from Bale Mountain lakes and the East African lake  
447 database, the best performing temperature calibration is a modified MBT<sub>SME</sub> including IIIa'.

448 With the use of the new calibration, the Garba Guracha MAT record reflects insolation variability as one of the main  
449 climatic drivers at millennial scales. Additional factors such as glacier and permafrost melting during deglaciation and  
450 the regional atmospheric circulation likely play a prominent role on shorter time scales. These additional mechanisms  
451 partly explain the asynchronicity between the Garba Guracha MAT record in the high altitude afro-alpine region of  
452 the Horn of Africa and other eastern African lake records.

453 Further research is necessary to understand the influences on and the origin of brGDGTs producing communities,  
454 especially at high altitudes.

455

456

457 **Author contribution.** LB, GGR, HFL, and MZ collected the samples. LB, CDJ, JMR and MZ developed the concept.  
458 LB and CDJ extracted, analyzed and interpreted the brGDGT data. LB led the manuscript writing with contributions  
459 and feedback from all authors. MZ acquired the funding and supervised the work.



460 **Competing interests.** The authors declare that they have no conflict of interest.

461 **Acknowledgements**

462 This research was funded by the German Research Council (DFG: ZE 844/10–1) in the framework of the joint Ethio-  
463 European DFG Research Unit 2358 "The Mountain Exile Hypothesis. How humans benefited from and reshaped  
464 African high-altitude ecosystems during Quaternary climate changes". We are grateful to the project coordination, the  
465 Philipps University Marburg, University of Addis Abeba, the Frankfurt Zoological Society, the Ethiopian Wolf Project,  
466 the Bale Mountains National Park, and the related staff members, especially Katinka Thielsen and Mekbib Fekadu for  
467 their logistic assistance during our fieldwork. We thank the Ethiopian Wildlife Conservation Authority for permitting  
468 our research in the Bale Mountains National Park.

469

470 **7. REFERENCES**

- 471 Alley, R. B.: The Younger Dryas cold interval as viewed from central Greenland, *Quaternary Science Reviews*, 19,  
472 213–226, [https://doi.org/https://doi.org/10.1016/S0277-3791\(99\)00062-1](https://doi.org/https://doi.org/10.1016/S0277-3791(99)00062-1), 2000.
- 473 Baxter, A. J., Hopmans, E. C., Russell, J. M., and Sinninghe Damsté, J. S.: Bacterial GMGTs in East African lake  
474 sediments: Their potential as palaeotemperature indicators, *Geochimica et Cosmochimica Acta*, 259, 155–169,  
475 <https://doi.org/10.1016/j.gca.2019.05.039>, 2019.
- 476 Berke, M. A., Johnson, T. C., Werne, J. P., Schouten, S., and Sinninghe Damsté, J. S.: A mid-Holocene thermal  
477 maximum at the end of the African Humid Period, *Earth and Planetary Science Letters*, 351–352, 95–104,  
478 <https://doi.org/10.1016/j.epsl.2012.07.008>, 2012a.
- 479 Berke, M. A., Johnson, T. C., Werne, J. P., Grice, K., Schouten, S., and Sinninghe Damsté, J. S.: Molecular records of  
480 climate variability and vegetation response since the Late Pleistocene in the Lake Victoria basin, East Africa,  
481 *Quaternary Science Reviews*, 55, 59–74, <https://doi.org/10.1016/j.quascirev.2012.08.014>, 2012b.
- 482 Bini, M., Zanchetta, G., Perşoiu, A., Cartier, R., Català, A., Cacho, I., Dean, J. R., Di Rita, F., Drysdale, R. N., Finnè,  
483 M., Isola, I., Jalali, B., Lirer, F., Magri, D., Masi, A., Marks, L., Mercuri, A. M., Peyron, O., Sadori, L., Sicre, M.-A.,  
484 Welc, F., Zielhofer, C., and Brisset, E.: The 4.2 ka BP Event in the Mediterranean region: an overview, *Clim. Past*, 15,  
485 555–577, <https://doi.org/10.5194/cp-15-555-2019>, 2019.
- 486 Bittner, L., Bliedner, M., Grady, D., Gil-Romera, G., Martin-Jones, C., Lemma, B., Mekonnen, B., Lamb, H. F., Yang,  
487 H., Glaser, B., Szidat, S., Salazar, G., Rose, N. L., Opgenoorth, L., Miehe, G., Zech, W., and Zech, M.: Revisiting



488 afro-alpine Lake Garba Guracha in the Bale Mountains of Ethiopia: rationale, chronology, geochemistry, and  
489 paleoenvironmental implications, *Journal of Paleolimnology*, <https://doi.org/10.1007/s10933-020-00138-w>, 2020.

490 Bittner, L., Gil-Romera, G., Grady, D., Lamb, H. F., Lorenz, E., Weiner, M., Meyer, H., Bromm, T., Glaser, B., and  
491 Zech, M.: The Holocene lake-evaporation history of the afro-alpine Lake Garba Guracha in the Bale Mountains,  
492 Ethiopia, based on  $\delta^{18}\text{O}$  records of sugar biomarker and diatoms, *Quaternary Research*, 1–14,  
493 <https://doi.org/10.1017/qua.2021.26>, 2021.

494 Blom, R. G., Farr, T. G., Feynmann, J., Ruzmaikin, A., and Paillou, P.: The green Sahara: Climate change, hydrologic  
495 history and human occupation, in: 2009 IEEE Radar Conference, 1–4, <https://doi.org/10.1109/RADAR.2009.4977129>,  
496 2009.

497 Bonnefille, R., Chalié, F., Guiot, J., and Vincens, A.: Quantitative estimates of full glacial temperatures in equatorial  
498 Africa from palynological data\*, *Climate Dynamics*, 6, 251–257, <https://doi.org/10.1007/BF00193538>, 1992.

499 van Bree, L. G. J., Peterse, F., Baxter, A. J., De Crop, W., van Grinsven, S., Villanueva, L., Verschuren, D., and  
500 Sinninghe Damsté, J. S.: Seasonal variability and sources of in situ brGDGT production in a permanently stratified  
501 African crater lake, *Biogeosciences Discuss.*, 2020, 1–36, <https://doi.org/10.5194/bg-2020-233>, 2020.

502 Castañeda, I. S., Schouten, S., Pätzold, J., Lucassen, F., Kasemann, S., Kuhlmann, H., and Schefuß, E.: Hydroclimate  
503 variability in the Nile River Basin during the past 28,000 years, *Earth and Planetary Science Letters*, 438, 47–56,  
504 <https://doi.org/10.1016/j.epsl.2015.12.014>, 2016.

505 Cheddadi, R., Lamb, H. F., Guiot, J., and van der Kaars, S.: Holocene climatic change in Morocco: a quantitative  
506 reconstruction from pollen data, *Climate Dynamics*, 14, 883–890, <https://doi.org/10.1007/s003820050262>, 1998.

507 Chevalier, M. and Chase, B. M.: Southeast African records reveal a coherent shift from high- to low-latitude forcing  
508 mechanisms along the east African margin across last glacial–interglacial transition, *Quaternary Science Reviews*, 125,  
509 117–130, <https://doi.org/10.1016/j.quascirev.2015.07.009>, 2015.

510 Costa, K., Russell, J., Konecky, B., and Lamb, H.: Isotopic reconstruction of the African Humid Period and Congo Air  
511 Boundary migration at Lake Tana, Ethiopia, *Quaternary Science Reviews*, 83, 58–67,  
512 <https://doi.org/10.1016/j.quascirev.2013.10.031>, 2014.

513 Damsté, J. S. S., Hopmans, E. C., Pancost, R. D., Schouten, S., and Geenevasen, J. A. J.: Newly discovered non-  
514 isoprenoid glycerol dialkyl glycerol tetraether lipids in sediments, *Chemical Communications*, 1683–1684,  
515 <https://doi.org/10.1039/b004517i>, 2000.

516 Dearing Crampton-Flood, E., Tierney, J. E., Peterse, F., Kirkels, F. M. S. A., and Sinninghe Damsté, J. S.: BayMBT:



- 517 A Bayesian calibration model for branched glycerol dialkyl glycerol tetraethers in soils and peats, *Geochimica et*  
518 *Cosmochimica Acta*, 268, 142–159, <https://doi.org/10.1016/j.gca.2019.09.043>, 2020.
- 519 Dee, S. G., Morrill, C., Kim, S. H., and Russell, J. M.: Hot Air, Hot Lakes, or Both? Exploring Mid-Holocene African  
520 Temperatures Using Proxy System Modeling, *Journal of Geophysical Research: Atmospheres*, 126, e2020JD033269,  
521 <https://doi.org/10.1029/2020JD033269>, 2021.
- 522 deMenocal, P., Ortiz, J., Guilderson, T., Adkins, J., Sarnthein, M., Baker, L., and Yarusinsky, M.: Abrupt onset and  
523 termination of the African Humid Period., *Quaternary Science Reviews*, 19, 347–361, [https://doi.org/10.1016/S0277-](https://doi.org/10.1016/S0277-3791(99)00081-5)  
524 [3791\(99\)00081-5](https://doi.org/10.1016/S0277-3791(99)00081-5), 2000.
- 525 Eggermont, Windafrash, M., Van Damme, M., Lens, K., and Umer M., H.: Bale Moluntains Lakes : Ecosystems under  
526 pressure of global change?, *Walia*, 2011, 171–180, [https://doi.org/10.10520/AJA00837059\\_148](https://doi.org/10.10520/AJA00837059_148), 2011.
- 527 Eggermont, H., Heiri, O., James, A., Ae, R., Vuille, M., Leen, A., Ae, A., and Verschuren, D.: Paleotemperature  
528 reconstruction in tropical Africa using fossil Chironomidae (Insecta: Diptera), *Journal of Paleolimnology*, 43, 413–  
529 435, <https://doi.org/10.1007/s10933-009-9339-2>, 2010.
- 530 Garelick, S., Russell, J., Richards, A., Smith, J., Kelly, M., Anderson, N., Jackson, M. S., Doughty, A., Nakileza, B.,  
531 Ivory, S., Dee, S., and Marshall, C.: The dynamics of warming during the last deglaciation in high-elevation regions  
532 of Eastern Equatorial Africa, *Quaternary Science Reviews*, 281, 107416,  
533 <https://doi.org/10.1016/j.quascirev.2022.107416>, 2022.
- 534 Gasse, F.: Hydrological changes in the African tropics since the Last Glacial Maximum, *Quaternary Science Reviews*,  
535 19, 189–211, [https://doi.org/10.1016/S0277-3791\(99\)00061-X](https://doi.org/10.1016/S0277-3791(99)00061-X), 2000.
- 536 Gil-Romera, G., Adolf, C., Benito Blas, M., Bittner, L., Johansson, M. M. U., Grady, D. D. A., Lamb, H. H. F., Lemma,  
537 B., Fekadu, M., Glaser, B., Mekonnen, B., Sevilla-Callejo, M., Zech, M., Zech, W., Miehe, G., Benito, B. M., Bittner,  
538 L., Johansson, M. M. U., Grady, D. D. A., Lamb, H. H. F., Lemma, B., Fekadu, M., Glaser, B., Mekonnen, B., Sevilla-  
539 Callejo, M., Zech, M., Zech, W., and Miehe, G.: Long-term fire resilience of the Ericaceous Belt, Bale Mountains,  
540 Ethiopia, *Biology Letters*, 15, 20190357, <https://doi.org/10.1098/rsbl.2019.0357>, 2019.
- 541 Gil-Romera, G., Fekadu, M., Opgenoorth, L., Grady, D., Lamb, H. F., Bittner, L., Zech, M., and Miehe, G.: The new  
542 Garba Guracha palynological sequence: Revision and data expansion, in: *Quaternary Vegetation Dynamics – The*  
543 *African Pollen Database*, edited by: Runge, J., Gosling, W.D., Lézine, A-M., S. L., CRC Press, London, 442,  
544 <https://doi.org/10.1201/9781003162766>, 2021.
- 545 Groos, A., Akçar, N., Yesilyurt, S., Miehe, G., Vockenhuber, C., and Veit, H.: Nonuniform Late Pleistocene glacier



- 546 fluctuations in tropical Eastern Africa, *Science Advances*, 7, <https://doi.org/10.1126/sciadv.abb6826>, 2021.
- 547 Groos, A. R., Niederhauser, J., Wraase, L., Hänsel, F., Nauss, T., Akçar, N., and Veit, H.: Implications of present  
548 ground temperatures and relict stone stripes in the Ethiopian Highlands for the palaeoclimate of the tropics, *Earth Surf.*  
549 *Dynam. Discuss.*, 2020, 1–37, <https://doi.org/10.5194/esurf-2020-53>, 2020.
- 550 Hillman, J.: The Bale Mountains National Park Area, Southeast Ethiopia, and Its Management, 253 pp.,  
551 <https://doi.org/10.2307/3673456>, 1988.
- 552 Hopmans, E. C., Weijers, J. W. H., Schefuß, E., Herfort, L., Sinninghe Damsté, J. S., and Schouten, S.: A novel proxy  
553 for terrestrial organic matter in sediments based on branched and isoprenoid tetraether lipids, *Earth and Planetary*  
554 *Science Letters*, 224, 107–116, <https://doi.org/10.1016/j.epsl.2004.05.012>, 2004.
- 555 Hopmans, E. C., Schouten, S., and Sinninghe Damsté, J. S.: The effect of improved chromatography on GDGT-based  
556 palaeoproxies, *Organic Geochemistry*, 93, 1–6, <https://doi.org/https://doi.org/10.1016/j.orggeochem.2015.12.006>,  
557 2016.
- 558 Hove, H., Echeverria, D., and Parry, J.-E.: Review of current and planned adaptation action: East Africa, International  
559 Institute for Sustainable Development, Winnipeg, 2011.
- 560 Hughes, A. C., Orr, M. C., Ma, K., Costello, M. J., Waller, J., Provoost, P., Yang, Q., Zhu, C., and Qiao, H.: Sampling  
561 biases shape our view of the natural world, *Ecography*, 44, 1259–1269,  
562 <https://doi.org/https://doi.org/10.1111/ecog.05926>, 2021.
- 563 Huguet, C., Kim, J. H., Damsté, J. S. S., and Schouten, S.: Reconstruction of sea surface temperature variations in the  
564 Arabian Sea over the last 23 kyr using organic proxies (TEX<sub>86</sub> and U<sub>37K'</sub>), *Paleoceanography*, 21,  
565 <https://doi.org/10.1029/2005PA001215>, 2006.
- 566 Huybers, P.: Early Pleistocene Glacial Cycles and the Integrated Summer Insolation Forcing, *Science* (New York,  
567 N.Y.), 313, 508–511, <https://doi.org/10.1126/science.1125249>, 2006.
- 568 IPCC: Climate Change 2021: The Physical Science Basis. Contribution of Working Group I to the Sixth Assessment  
569 Report of the Intergovernmental Panel on Climate Change [Masson-Delmotte, V., P. Zhai, A. Pirani, S.L. Connors, C.  
570 Péan, S. Berger, N. Caud, Y. Chen, Cambridge University Press, 2021.
- 571 Ivory, S. J. and Russell, J.: Lowland forest collapse and early human impacts at the end of the African Humid Period  
572 at Lake Edward, equatorial East Africa, *Quaternary Research*, 89, 7–20, <https://doi.org/10.1017/qua.2017.48>, 2018.
- 573 Jaeschke, A., Thienemann, M., Schefuß, E., Urban, J., Schäbitz, F., Wagner, B., and Rethemeyer, J.: Holocene  
574 Hydroclimate Variability and Vegetation Response in the Ethiopian Highlands (Lake Dendi), *Frontiers in Earth*



- 575 Science, 8, 1–14, <https://doi.org/10.3389/feart.2020.585770>, 2020.
- 576 De Jonge, C., Hopmans, E. C., Zell, C. I., Kim, J.-H., Schouten, S., and Sinninghe Damsté, J. S.: Occurrence and  
577 abundance of 6-methyl branched glycerol dialkyl glycerol tetraethers in soils: Implications for palaeoclimate  
578 reconstruction, *Geochimica et Cosmochimica Acta*, 141, 97–112, <https://doi.org/10.1016/j.gca.2014.06.013>, 2014.
- 579 De Jonge, C., Radujković, D., Sigurdsson, B. D., Weedon, J. T., Janssens, I., and Peterse, F.: Lipid biomarker  
580 temperature proxy responds to abrupt shift in the bacterial community composition in geothermally heated soils,  
581 *Organic Geochemistry*, 137, <https://doi.org/10.1016/j.orggeochem.2019.07.006>, 2019.
- 582 De Jonge, C., Kuramae, E. E., Radujković, D., Weedon, J. T., Janssens, I. A., and Peterse, F.: The influence of soil  
583 chemistry on branched tetraether lipids in mid- and high latitude soils: Implications for brGDGT- based  
584 paleothermometry, *Geochimica et Cosmochimica Acta*, 310, 95–112,  
585 <https://doi.org/https://doi.org/10.1016/j.gca.2021.06.037>, 2021.
- 586 Junginger, A., Roller, S., Olaka, L. A., and Trauth, M. H.: The effects of solar irradiation changes on the migration of  
587 the Congo Air Boundary and water levels of paleo-Lake Suguta , Northern Kenya Rift , during the African Humid  
588 Period (15 – 5 ka BP), *Palaeogeography, Palaeoclimatology, Palaeoecology*, 396, 1–16,  
589 <https://doi.org/10.1016/j.palaeo.2013.12.007>, 2014.
- 590 Kassambara, A. and Mundt, F.: factoextra: Extract and Visualize the Results of Multivariate Data Analyses,  
591 <https://cran.r-project.org/package=factoextra>, 2020.
- 592 Kidane, Y., Stahlmann, R., and Beierkuhnlein, C.: Vegetation dynamics, and land use and land cover change in the  
593 Bale Mountains, Ethiopia, *Environmental Monitoring and Assessment*, 184, 7473–7489,  
594 <https://doi.org/10.1007/s10661-011-2514-8>, 2012.
- 595 Laskar, J., Robutel, P., Joutel, F., Gastineau, M., Correia, A. C. M., and Levrard, B.: A long-term numerical solution  
596 for the insolation quantities of the Earth , *A&A*, 428, 261–285, 2004.
- 597 Löffler, H.: Limnology and paleolimnological data on the Bale Mountain Lakes, Verth, International Verein.  
598 *Limnology*, 20, 1131–1138, 1978.
- 599 Loomis, S. E., Russell, J. M., and Sinninghe Damsté, J. S.: Distributions of branched GDGTs in soils and lake  
600 sediments from western Uganda: Implications for a lacustrine paleothermometer, *Organic Geochemistry*, 42, 739–751,  
601 <https://doi.org/10.1016/j.orggeochem.2011.06.004>, 2011.
- 602 Loomis, S. E., Russell, J. M., Heures, A. M., D’Andrea, W. J., and Sinninghe Damsté, J. S.: Seasonal variability of  
603 branched glycerol dialkyl glycerol tetraethers (brGDGTs) in a temperate lake system, *Geochimica et Cosmochimica*



- 604 Acta, 144, 173–187, <https://doi.org/10.1016/j.gca.2014.08.027>, 2014.
- 605 Loomis, S. E., Russell, J. M., and Lamb, H. F.: Northeast African temperature variability since the Late Pleistocene,  
606 Palaeogeography, Palaeoclimatology, Palaeoecology, 423, 80–90, <https://doi.org/10.1016/j.palaeo.2015.02.005>, 2015.
- 607 Loomis, S. E., Russell, J. M., Verschuren, D., Morrill, C., De Cort, G., Sinninghe Damsté, J. S., Olago, D., Eggermont,  
608 H., Street-Perrott, F. A., and Kelly, M. A.: The tropical lapse rate steepened during the Last Glacial Maximum, Science  
609 Advances, 3, <https://doi.org/10.1126/sciadv.1600815>, 2017.
- 610 Loomis, S. E. S. E., Russell, J. M., Ladd, B., Street-Perrott, F. A. A., and Sinninghe Damsté, J. S. J. S.: Calibration  
611 and application of the branched GDGT temperature proxy on East African lake sediments, Earth and Planetary Science  
612 Letters, 357–358, 277–288, <https://doi.org/https://doi.org/10.1016/j.epsl.2012.09.031>, 2012.
- 613 Lyon, B. and Vigaud, N.: Unraveling East Africa’s Climate Paradox,  
614 <https://doi.org/https://doi.org/10.1002/9781119068020.ch16>, 22 June 2017.
- 615 Marshall, M., Lamb, H., Davies, S., Leng, M., Bedaso, Z., Umer, M., and Bryant, C.: Climatic change in northern  
616 Ethiopia during the past 17,000 years: A diatom and stable isotope record from Lake Ashenge, Palaeogeography  
617 Palaeoclimatology Palaeoecology, 279, <https://doi.org/10.1016/j.palaeo.2009.05.003>, 2009.
- 618 Martínez-Sosa, P., Tierney, J. E., Stefanescu, I. C., Crampton-Flood, E. D., Shuman, B. N., and Routson, C.: A global  
619 Bayesian temperature calibration for lacustrine brGDGTs, <https://doi.org/10.1594/PANGAEA.931169>, 6 May 2021.
- 620 Mische, S. and Mische, G.: Ericaceous forests and heathlands in the Bale mountains of South Ethiopia : ecology and  
621 man’s impact, edited by: Mische, G. and 1952-, Reinbek : Warnke, Reinbek, 1994.
- 622 Morrissey, A. and Scholz, C. A. C. A. C. A.: Paleohydrology of Lake Turkana and its influence on the Nile River  
623 system, Palaeogeography, Palaeoclimatology, Palaeoecology, 403, 88–100,  
624 <https://doi.org/https://doi.org/10.1016/j.palaeo.2014.03.029>, 2014.
- 625 Morrissey, A., Scholz, C. A., and Russell, J. M.: Late Quaternary TEX<sub>86</sub> paleotemperatures from the world’s largest  
626 desert lake, Lake Turkana, Kenya, Journal of Paleolimnology, 59, 103–117, [https://doi.org/10.1007/s10933-016-9939-](https://doi.org/10.1007/s10933-016-9939-6)  
627 6, 2018.
- 628 Neukom, R., Barboza, L. A., Erb, M. P., Shi, F., Emile-Geay, J., Evans, M. N., Franke, J., Kaufman, D. S., Lücke, L.,  
629 Rehfeld, K., Schurer, A., Zhu, F., Brönnimann, S., Hakim, G. J., Henley, B. J., Ljungqvist, F. C., McKay, N., Valler,  
630 V., von Gunten, L., and Consortium, P. 2k: Consistent multidecadal variability in global temperature reconstructions  
631 and simulations over the Common Era, Nature Geoscience, 12, 643–649, <https://doi.org/10.1038/s41561-019-0400-0>,  
632 2019.



- 633 Nicholson, S. E.: Climate and climatic variability of rainfall over eastern Africa, *Reviews of Geophysics*, 55, 590–635,  
634 <https://doi.org/https://doi.org/10.1002/2016RG000544>, 2017.
- 635 Osmaston, H. A., Mitchell, W. A., and Osmaston, J. A. N.: Quaternary glaciation of the Bale Mountains, Ethiopia,  
636 *Journal of Quaternary Science*, 20, 593–606, <https://doi.org/10.1002/jqs.931>, 2005.
- 637 Ossendorf, G., Groos, A., Bromm, T., Girma Tekelemariam, M., Glaser, B., Lesur, J., Schmidt, J., Akçar, N., Bekele,  
638 T., Beldados, A., Demissew, S., Hadush Kahsay, T., P Nash, B., Nauss, T., Negash, A., Nemomissa, S., Veit, H.,  
639 Vogelsang, R., Zerihun, W., and Mieke, G.: Middle Stone Age foragers resided in high elevations of the glaciated Bale  
640 Mountains, Ethiopia, *Science*, 365, 583–587, 2019.
- 641 Otto-Bliesner, B. L., Russell, J. M., Clark, P. U., Liu, Z., Overpeck, J. T., Konecky, B., DeMenocal, P., Nicholson, S.  
642 E., He, F., and Lu, Z.: Coherent changes of south-eastern equatorial and northern African rainfall during the last  
643 deglaciation, *Science*, 346, 1223–1227, <https://doi.org/10.1126/science.1259531>, 2014.
- 644 Peterse, F., van der Meer, J., Schouten, S., Weijers, J. W. H., Fierer, N., Jackson, R. B., Kim, J.-H., and Sinninghe  
645 Damsté, J. S.: Revised calibration of the MBT–CBT paleotemperature proxy based on branched tetraether membrane  
646 lipids in surface soils, *Geochimica et Cosmochimica Acta*, 96, 215–229,  
647 <https://doi.org/https://doi.org/10.1016/j.gca.2012.08.011>, 2012.
- 648 Powers, L. A., Johnson, T. C., Werne, J. P., Castañeda, I. S., Hopmans, E. C., Sinninghe Damsté, J. S., and Schouten,  
649 S.: Large temperature variability in the southern African tropics since the Last Glacial Maximum, *Geophysical*  
650 *Research Letters*, 32, 1–4, <https://doi.org/10.1029/2004GL022014>, 2005.
- 651 R Core Team: R: A Language and Environment for Statistical Computing, <https://www.r-project.org/>, 2021.
- 652 Raberg, J. H., Harning, D. J., Crump, S. E., de Wet, G., Blumm, A., Kopf, S., Geirsdóttir, Á., Miller, G. H., and  
653 Sepúlveda, J.: Revised fractional abundances and warm-season temperatures substantially improve brGDGT  
654 calibrations in lake sediments, *Biogeosciences*, 18, 3579–3603, <https://doi.org/10.5194/bg-18-3579-2021>, 2021.
- 655 Russell, J. M., Hopmans, E. C., Loomis, S. E., Liang, J., and Sinninghe Damsté, J. S.: Distributions of 5- and 6-methyl  
656 branched glycerol dialkyl glycerol tetraethers (brGDGTs) in East African lake sediment: Effects of temperature, pH,  
657 and new lacustrine paleotemperature calibrations, *Organic Geochemistry*, 117, 56–69,  
658 <https://doi.org/10.1016/j.orggeochem.2017.12.003>, 2018.
- 659 Schouten, S., Forster, A., Panoto, F. E., and Sinninghe Damsté, J. S.: Towards calibration of the TEX<sub>86</sub>  
660 palaeothermometer for tropical sea surface temperatures in ancient greenhouse worlds, *Organic Geochemistry*, 38,  
661 1537–1546, <https://doi.org/10.1016/j.orggeochem.2007.05.014>, 2007.



- 662 Schreuder, L. T., Beets, C. J., Prins, M. A., Hatté, C., and Peterse, F.: Late Pleistocene climate evolution in Southeastern  
663 Europe recorded by soil bacterial membrane lipids in Serbian loess, *Palaeogeography, Palaeoclimatology,*  
664 *Palaeoecology*, 449, 141–148, <https://doi.org/10.1016/j.palaeo.2016.02.013>, 2016.
- 665 Sinninghe Damsté, J. S., Rijpstra, W. I. C., Foesel, B. U., Huber, K. J., Overmann, J., Nakagawa, S., Kim, J. J.,  
666 Dunfield, P. F., Dedysh, S. N., and Villanueva, L.: An overview of the occurrence of ether- and ester-linked iso-  
667 diabolic acid membrane lipids in microbial cultures of the Acidobacteria: Implications for brGDGT paleoproxies for  
668 temperature and pH, *Organic Geochemistry*, 124, 63–76, <https://doi.org/10.1016/j.orggeochem.2018.07.006>, 2018.
- 669 Tiercelin, J. J., Gibert, E., Umer, M., Bonnefille, R., Disnar, J. R., Lézine, A. M., Hureau-Mazaudier, D., Travi, Y.,  
670 Keravis, D., and Lamb, H. F.: High-resolution sedimentary record of the last deglaciation from a high-altitude lake in  
671 Ethiopia, *Quaternary Science Reviews*, 27, 449–467, <https://doi.org/10.1016/j.quascirev.2007.11.002>, 2008.
- 672 Tierney, J. E. and deMenocal, P. B.: Abrupt Shifts in Horn of Africa Hydroclimate Since the Last Glacial Maximum,  
673 *Science*, 342, 843–846, <https://doi.org/10.1126/science.1240411>, 2013.
- 674 Tierney, J. E. and Russell, J. M.: Abrupt climate change in southeast tropical Africa influenced by Indian monsoon  
675 variability and ITCZ migration, *Geophysical Research Letters*, 34, <https://doi.org/10.1029/2007GL029508>, 2007.
- 676 Tierney, J. E., Russell, J. M., Huang, Y., Damsté, J. S. S., Hopmans, E. C., and Cohen, A. S.: Northern Hemisphere  
677 Controls on Tropical Southeast African Climate During the Past 60,000 Years, *Science*, 322, 252–255,  
678 <https://doi.org/10.1126/science.1160485>, 2008.
- 679 Tierney, J. E., Russell, J. M., Sinninghe Damsté, J. S., Huang, Y., and Verschuren, D.: Late Quaternary behavior of  
680 the East African monsoon and the importance of the Congo Air Boundary, *Quaternary Science Reviews*, 30, 798–807,  
681 <https://doi.org/10.1016/j.quascirev.2011.01.017>, 2011a.
- 682 Tierney, J. E., Lewis, S. C., Cook, B. I., LeGrande, A. N., and Schmidt, G. A.: Model, proxy and isotopic perspectives  
683 on the East African Humid Period, *Earth and Planetary Science Letters*, 307, 103–112,  
684 <https://doi.org/10.1016/j.epsl.2011.04.038>, 2011b.
- 685 Tierney, J. E., Smerdon, J. E., Anchukaitis, K. J., and Seager, R.: Multidecadal variability in East African hydroclimate  
686 controlled by the Indian Ocean, *Nature*, 493, 389–392, <https://doi.org/10.1038/nature11785>, 2013.
- 687 Tierney, J. E., Pausata, F. S. R., and Demenocal, P.: Deglacial Indian monsoon failure and North Atlantic stadials  
688 linked by Indian Ocean surface cooling, *Nature Geoscience*, 9, 46–50, <https://doi.org/10.1038/ngeo2603>, 2016.
- 689 Tierney, J. E., Pausata, F. S. R., and DeMenocal, P. B.: Rainfall regimes of the Green Sahara, *Science Advances*, 3,  
690 <https://doi.org/10.1126/sciadv.1601503>, 2017.



- 691 Trauth, M. H., Foerster, V., Junginger, A., Asrat, A., Lamb, H. F., and Schaebitz, F.: Abrupt or gradual? Change point  
692 analysis of the late Pleistocene–Holocene climate record from Chew Bahir, southern Ethiopia, *Quaternary Research*,  
693 90, 321–330, <https://doi.org/DOI: 10.1017/qua.2018.30>, 2018.
- 694 Uhlig, S. and Uhlig, K.: Studies on the Altitudinal Zonation of Forests and Alpine Plants in the Central Bale Mountains,  
695 Ethiopia, 153 pp., <https://doi.org/10.2307/3673574>, 1991.
- 696 Uhlig, S. K.: Mountain Forests and the Upper Tree Limit on the Southeastern Plateau of Ethiopia, *Mountain Research*  
697 *and Development*, 8, 227–234, <https://doi.org/10.2307/3673452>, 1988.
- 698 Umer, M., Lamb, H. F., Bonnefille, R., Lézine, A. M., Tiercelin, J. J., Gibert, E., Cazet, J. P., and Watrin, J.: Late  
699 Pleistocene and Holocene vegetation history of the Bale Mountains, Ethiopia, *Quaternary Science Reviews*, 26, 2229–  
700 2246, <https://doi.org/10.1016/j.quascirev.2007.05.004>, 2007.
- 701 Wagner, B., Wennrich, V., Viehberg, F., Junginger, A., Kolvenbach, A., Rethemeyer, J., Schaebitz, F., and Schmiedl,  
702 G.: Holocene rainfall runoff in the central Ethiopian highlands and evolution of the River Nile drainage system as  
703 revealed from a sediment record from Lake Dendi, *Global and Planetary Change*, 163, 29–43,  
704 <https://doi.org/10.1016/j.gloplacha.2018.02.003>, 2018.
- 705 Weber, Y., Damsté, J. S. S., Zopfi, J., De Jonge, C., Gilli, A., Schubert, C. J., Lepori, F., Lehmann, M. F., and Niemann,  
706 H.: Redox-dependent niche differentiation provides evidence for multiple bacterial sources of glycerol tetraether lipids  
707 in lakes, *Proceedings of the National Academy of Sciences of the United States of America*, 115, 10926–10931,  
708 <https://doi.org/10.1073/pnas.1805186115>, 2018.
- 709 Weijers, J. W. H., Schefuß, E., Schouten, S., and Damsté, J. S. S.: Coupled thermal and hydrological evolution of  
710 tropical Africa over the last deglaciation, *Science*, 315, 1701–1704, <https://doi.org/10.1126/science.1138131>, 2007a.
- 711 Weijers, J. W. H., Schouten, S., van den Donker, J. C., Hopmans, E. C., and Sinninghe Damsté, J. S.: Environmental  
712 controls on bacterial tetraether membrane lipid distribution in soils, *Geochimica et Cosmochimica Acta*, 71, 703–713,  
713 <https://doi.org/10.1016/j.gca.2006.10.003>, 2007b.
- 714 Werdecker, J.: Eine Durchquerung des Goba-Massivs in Südäthiopien, *Hermann vo*, 132–144, 1962.
- 715 Williams, F. M.: *The Southeastern Highlands and the Ogaden*, edited by: Williams, F. M., Springer International  
716 Publishing, Cham, 153–170, [https://doi.org/10.1007/978-3-319-02180-5\\_15](https://doi.org/10.1007/978-3-319-02180-5_15), 2016.
- 717 Woldu, Z., Feoli, E., and Nigatu, L.: Partitioning an elevation gradient of vegetation from south-eastern Ethiopia by  
718 probabilistic methods, *Plant Ecology*, 81, 189–198, 1989.
- 719 Wu, H., Guiot, J., Brewer, S., and Guo, Z.: Climatic changes in Eurasia and Africa at the last glacial maximum and



720 mid-Holocene: reconstruction from pollen data using inverse vegetation modelling, *Climate Dynamics*, 29, 211–229,

721 <https://doi.org/10.1007/s00382-007-0231-3>, 2007.

722 Zeng, F. and Yang, H.: Temperature changes reconstructed from branched GDGTs on the central Loess Plateau during

723 the past 130–5 ka, *Quaternary International*, 503, 3–9, <https://doi.org/https://doi.org/10.1016/j.quaint.2018.04.045>,

724 2019.

725

726

727

728

729

730

731

732

733

734

735

736

737